CrossMark

J. Fluid Mech. (2017), *vol.* 819, *pp.* 147–164. © Cambridge University Press 2017
doi:10.1017/jfm.2017.167

Towards a quantitative comparison between global and local stability analysis

L. Siconolfi[1], V. Citro[2], F. Giannetti[2,†], S. Camarri[1] and P. Luchini[2]

[1]DICI, Università di Pisa, Via Girolamo Caruso, 56122 Pisa, Italy

[2]DIIN, Universitá degli Studi di Salerno, Via Giovanni Paolo II, 84084 Fisciano (SA), Italy

(Received 1 June 2016; revised 11 March 2017; accepted 11 March 2017;
first published online 18 April 2017)

A methodology is proposed here to estimate the stability characteristics of bluff-body wakes using local analysis under the assumption of weakly non-parallel flows. In this connection, a generalisation of the classic spatio-temporal stability analysis for fully three-dimensional flows is first described. Secondly, an additional higher-order correction term with respect to the common saddle-point global frequency estimation is included in the analysis. The proposed method is first validated for the case of the flow past a circular cylinder and then applied to two fully three-dimensional flows: the boundary layer flow over a wall-mounted hemispherical body and the wake flow past a fixed sphere. In all the cases considered, both the estimated unstable eigenvalue and the spatial shape of the associated eigenmode are determined by local stability analysis, and they are compared with the reference counterparts obtained at a definitely higher computational cost by a fully three-dimensional global stability analysis. It is shown that the results of local stability analysis, when the higher-order correction term is included, are in excellent agreement with those obtained by global stability analysis. It is also shown that the retained correction term is of crucial importance in this perspective, leading to a remarkable improvement in accuracy with respect to the classical saddle-point estimation.

Key words: absolute/convective instability, instability, wakes

1. Introduction

Spatially developing open flows such as bluff-body wakes or jets may behave as global oscillators due to an intrinsically unsteady dynamics which drives self-sustained oscillations. In order to investigate the dynamic behaviour of these flows the fundamental concept of local absolute frequency ω_0 has been introduced (Briggs 1964; Bers 1983). In the regions of absolute instability, i.e. $\omega_{0,i} \equiv \mathrm{Im}(\omega_0) > 0$ (Im(·) indicating the imaginary part of a complex number), the perturbations are not convected downstream, but they grow in place, driving the successive evolution of the flow. In particular, when a sufficiently large region of absolute instability develops, a self-sustained resonance occurs which can be detected and identified by a global stability analysis of the flow (see Huerre & Monkewitz 1985; Chomaz, Huerre & Redekopp 1988; Monkewitz, Huerre & Chomaz 1993).

† Email address for correspondence: fgiannetti@unisa.it

https://doi.org/10.1017/jfm.2017.167 Published online by Cambridge University Press

In this context, the dynamics of perturbations can be analysed both from a local and a global point of view. In the local stability analysis, under the assumption of weakly non-parallel flows, small-amplitude waves are considered as perturbations of a given base flow and their dynamics is studied by carrying out a separate analysis for each streamwise station included in the analysis. On the other hand, in global stability analysis the temporal evolution of perturbations in the flow domain is investigated at once and the spatial shape of the most unstable perturbations is a result of the analysis. In the past, several works have been devoted to investigating the relationship between the global stability characteristics and the local ones for different flow configurations (see, e.g. Pier 2002; Juniper, Tammisola & Lundell 2011). For instance, in the reviews by Huerre & Monkewitz (1990) and in Huerre & Rossi (1998), the occurrence of a globally unstable mode is identified in terms of the local properties of the flow field using the classical WKBJ (Wentzel–Kramers–Brillouin–Jeffrey) asymptotic analysis (see Bender & Orszag 1978). Particular attention was devoted to clarifying the role of the region of absolute instability in the generation of an unstable global mode and, related to this, to the identification, still in the context of the local analysis, of the complex spatial position where the flow is most sensitive to changes in the internal feedback mechanism, usually referred to as the wavemaker.

The possibility of approximating the results of a global stability analysis by using a local approach leads to a substantial saving of the computational time and of the required computer resources, since the eigenvalue problem related to the discretisation of the global stability problem over the whole domain is replaced by a set of independent small-size eigenvalue problems. This aspect is particularly attractive when fully three-dimensional flows are investigated, as the computational resources required for the global stability analysis of such flows is at the state of the art of both computational methods and resources. However, the use of the WKBJ approximation can be justified for base flows that evolve slowly in space in comparison with the typical wavelength of the instability in that direction. Nevertheless, this approximation has been successfully applied even beyond the limit of its validity, as may happen in bluff-body wakes. For example, Giannetti & Luchini (2007) showed a qualitative agreement between the linear global and local stability analysis for the case of the flow past a circular cylinder, for Reynolds numbers (Re) ranging from 5 to 100 (based on the incoming velocity and diameter of the cylinder). Subsequently, Pier (2008) considered the flow past a fixed sphere, where the local stability features are obtained under a quasi-parallel flow assumption. Lastly, Juniper & Pier (2015) showed that a local analysis can be used also for the identification of the adjoint modes and for structural sensitivity, showing the results for a slowly developing confined wake and for the flow past a circular cylinder at $Re = 50$. In all of the previously mentioned studies the resulting eigenvalues computed by a local approach can be used mainly for a qualitative analysis since, in general, the inherent errors in comparison with the reference global solutions (growth rate, frequency and mode structure) can be significant.

In this context, our aim is to show that by including a higher-order corrective term of the WKBJ approximation, which is neglected in the classical spatio-temporal analysis, the local approach can be used to provide a quantitative estimation of the global eigenvalue related to the wake self-sustained instability and of the corresponding eigenmode. Furthermore, we also show that a two-dimensional local analysis can be used to study fully three-dimensional wakes by a natural generalisation of the classical spatio-temporal stability analysis. In conclusion, we stress that such a two-dimensional local approach is orders of magnitude cheaper in terms

https://doi.org/10.1017/jfm.2017.167 Published online by Cambridge University Press

of computational costs than the global three-dimensional modal analysis, and for this reason it can be considered as a valid alternative for studying fully three-dimensional flow configurations.

The paper is organised as follows. In § 2 the basic concepts of the global and local are summarised, together with the main results of the WKBJ approximation. The numerical techniques used in this paper are briefly described in § 3, while in § 4 the main results are presented in detail.

2. Theoretical framework

Let us consider a three-dimensional flow of a viscous fluid described by the unsteady incompressible Navier–Stokes equations. The equations, normalised using generic reference length ℓ and velocity U, are written as follows:

$$\boldsymbol{\nabla}\cdot\boldsymbol{u}=0, \tag{2.1a}$$

$$\frac{\partial \boldsymbol{u}}{\partial t}+\boldsymbol{u}\cdot\boldsymbol{\nabla}\boldsymbol{u}=-\boldsymbol{\nabla}p+\frac{1}{Re}\nabla^2\boldsymbol{u}, \tag{2.1b}$$

where $\boldsymbol{u}=(u, v, w)$ is the non-dimensional velocity field, p is the reduced pressure and $Re=U\ell\nu^{-1}$ is the flow Reynolds number, ν being the kinematic viscosity of the fluid. The system (2.1) is completed with appropriate boundary conditions specifying the particular configuration considered. The investigation of the instability mechanism acting on a given flow relies on the identification of a stationary solution $\boldsymbol{Q}_b=[\boldsymbol{U}_b, P_b]$ of the system (2.1), usually referred as base flow. Successively, the stability of the base flow can be investigated by different approaches depending on its characteristics (for a review, see Theofilis 2011).

2.1. *Global stability analysis*

When no assumptions can be made on the spatial structure of the base flow, a global stability analysis has to be considered in order to take into account the three-dimensional flow inhomogeneities. Here, the stability properties of the system are studied by considering the asymptotic behaviour in time of a generic small-amplitude perturbation $\boldsymbol{q}'=[\boldsymbol{u}', p'](x, y, z, t)$ superimposed on a base flow $\boldsymbol{Q}_b$. The evolution of the small-amplitude perturbation $\boldsymbol{q}'$ is described by the linearised Navier–Stokes equations, which are written as follows:

$$\boldsymbol{\nabla}\cdot\boldsymbol{u}'=0, \tag{2.2a}$$

$$\frac{\partial \boldsymbol{u}'}{\partial t}+\mathcal{L}_{Q_b}\{\boldsymbol{U}_b, Re\}\boldsymbol{u}'=-\boldsymbol{\nabla}p', \tag{2.2b}$$

where the linear operator $\mathcal{L}_{Q_b}$ is defined as:

$$\mathcal{L}_{Q_b}\{\boldsymbol{U}_b, Re\}\boldsymbol{u}'=\boldsymbol{U}_b\cdot\boldsymbol{\nabla}\boldsymbol{u}'+\boldsymbol{u}'\cdot\boldsymbol{\nabla}\boldsymbol{U}_b-\frac{1}{Re}\nabla^2\boldsymbol{u}'. \tag{2.3}$$

The system (2.2) has to be completed with appropriate homogeneous boundary conditions, which derive from the boundary conditions applied to the base flow. A non-trivial solution of the system (2.2) is usually sought in the classical normal mode form $\boldsymbol{q}'=\hat{\boldsymbol{q}}(x, y, z)\ \exp\{-\mathrm{i}\omega_G t\}$. When the disturbance written in normal form is then substituted in (2.2) a generalised eigenvalue problem in ω_G is obtained, whose solution indicates the global stability properties of the base flow.

https://doi.org/10.1017/jfm.2017.167 Published online by Cambridge University Press

2.2. *WKBJ asymptotic approximation*

When the base flow, described here in Cartesian coordinates (x, y, z), slowly evolves in a given direction, (assumed to be aligned with the x axis), a local linear stability analysis can be performed within a WKBJ framework. In this context, the perturbation $\boldsymbol{q}'(x, y, z, t)$ of the base flow is sought in the following form:

$$\boldsymbol{q}' = [\boldsymbol{u}', P'](x, y, z, t) = \mathrm{e}^{\mathrm{i}(\phi(X)/\epsilon - \omega t)} \sum_n \boldsymbol{q}'_n(X, y, z)\epsilon^n, \tag{2.4}$$

where $X = \epsilon x$ is the slow streamwise variable on which the base flow depends, $\phi(X)$ is a phase function whose derivative represents the spatial wavenumber k ($k(X) = \mathrm{d}\phi(X)/\mathrm{d}X$) and ϵ is a small parameter indicating the ratio between the characteristic instability wavelength $\lambda = 2\pi/k$ and the characteristic spatial length scale L over which the base flow $\boldsymbol{Q}_b(X, y, z)$ experiences an $O(1)$ change (Huerre & Monkewitz 1990). By collecting terms according to their scaling with ϵ, we obtain a series of problems. At leading order $O(\epsilon^0)$, the following equations are retrieved:

$$\mathrm{i}k\hat{u} + \frac{\partial \hat{v}}{\partial y} + \frac{\partial \hat{w}}{\partial z} = 0, \tag{2.5a}$$

$$\mathrm{i}\hat{u}\frac{\partial U_b}{\partial x} - U_b k\hat{u} + \xi\hat{u} + \mathrm{i}\hat{v}\frac{\partial U_b}{\partial y} + \mathrm{i}\hat{w}\frac{\partial U_b}{\partial z} - k\hat{p} + \frac{\mathrm{i}k^2}{Re}\hat{u} = -\omega\hat{u}, \tag{2.5b}$$

$$-U_b k\hat{v} + \xi\hat{v} + \mathrm{i}\hat{v}\frac{\partial V_b}{\partial y} + \mathrm{i}\hat{w}\frac{\partial V_b}{\partial z} + \mathrm{i}\frac{\partial \hat{p}}{\partial y} + \frac{\mathrm{i}k^2}{Re}\hat{v} = -\omega\hat{v}, \tag{2.5c}$$

$$-U_b k\hat{w} + \xi\hat{w} + \mathrm{i}\hat{v}\frac{\partial W_b}{\partial y} + \mathrm{i}\hat{w}\frac{\partial W_b}{\partial z} + \mathrm{i}\frac{\partial \hat{p}}{\partial z} + \frac{\mathrm{i}k^2}{Re}\hat{w} = -\omega\hat{w}, \tag{2.5d}$$

where

$$\xi = \left[\mathrm{i}V_b\frac{\partial}{\partial y} + \mathrm{i}W_b\frac{\partial}{\partial z} - \frac{\mathrm{i}}{Re}\left(\frac{\partial^2}{\partial y^2} + \frac{\partial^2}{\partial z^2}\right)\right]. \tag{2.6}$$

Note that in (2.5) we have also retained terms that are formally $O(\epsilon^1)$, such as those containing the streamwise derivative of the horizontal base flow component $\partial U_b/\partial x$, the cross-stream base flow velocity components V_b and W_b and the viscous perturbation terms. Here, in fact, we make use of a composite asymptotic expansion which is uniformly valid across the cross-stream plane, rather than using a rational asymptotic expansion (or multi-deck expansion). From a theoretical point of view, the minimal composite regular problem can be obtained by retaining at leading order only those $O(\epsilon^1)$ terms which contain a second derivative of a fluctuating quantity (i.e. the viscous perturbation terms). This choice produces the same set of equations used to study the stability of a purely parallel flow. However, keeping other $O(\epsilon^1)$ terms in the $O(\epsilon^0)$ problem does not invalidate the composite set of differential equations. Obviously, the leading-order problem arising from a composite expansion is not unique: moving terms from lower to higher order, in fact, does not affect the validity or the order of accuracy of the approximation, but modifies the form of the equations to be solved at different levels. In the present paper, we decided to retain all possible $O(\epsilon^1)$ terms, since their inclusion simplifies the numerical evaluation of the global frequency correction, as also explained later. Equations (2.5), together with homogeneous boundary conditions deriving from the conditions applied to the

https://doi.org/10.1017/jfm.2017.167 Published online by Cambridge University Press

base flow, represent an eigenvalue problem which characterises the local stability properties of the base flow at each considered streamwise section X. In particular, the wavenumber k and the frequency ω are linked by a dispersion relation which can be formally written as $D[k, \omega; X, Re] = 0$. For each streamwise location X and value of the Reynolds number, the dispersion relation couples the spatial structure of the eigenfunctions with their temporal behaviour.

A connection between the local stability characteristics provided by (2.5) and the global properties of the instability can be found by considering the higher-order terms of the WKBJ expansion (2.4). Here we just summarise the procedure and refer the interested reader to the seminal work by Huerre & Monkewitz (1990). Once the dispersion relation $D[k, \omega; X, Re] = 0$ is obtained (in the following the dependence on Re is omitted for brevity), the saddle point in the complex k-plane at each streamwise station X is determined to identify the absolute complex eigenvalue $\omega_0(X) = \omega(k_0; X)$, such that $\partial\omega/\partial k(k_0; X) = 0$. The existence of a finite region where the absolute growth rate $\omega_{0,i} > 0$, i.e. $\omega_{0,i} = \mathrm{Im}(\omega_0(X))$, is a necessary condition for the onset of self-sustained global oscillations (Chomaz *et al.* 1988). Considering a double infinite flow domain and under the assumption of the regularity of the dispersion relation $D[k, \omega; X] = 0$, the unknown global eigenvalue ω_G can be written as (Monkewitz *et al.* 1993):

$$\omega_G = \omega_s + \epsilon\omega_\epsilon, \tag{2.7}$$

where $\omega_s = \omega_0(X_s)$, X_s is the complex saddle point, or second-order turning point, such that $\partial\omega_0/\partial X(X_s) = 0$ and $\epsilon\omega_\epsilon$ is a small high-order correction term. Once ω_G has been identified at leading order, thus neglecting the term $\epsilon\omega_\epsilon$, the distribution of the direct global mode $\hat{\boldsymbol{q}}(x, y, z)$ can be expressed as follows in the region away from the turning point X_s:

$$\hat{\boldsymbol{q}}(x, y, z) \sim A^{\mp}(X)\hat{\boldsymbol{q}}(y, z; X) \exp\left[\mathrm{i}\epsilon^{-1}\int_{X_s}^{X} k^{\mp}(\omega_s; X')\,\mathrm{d}X'\right], \tag{2.8}$$

where $A(X)$ is a slowly evolving amplitude, $\hat{\boldsymbol{q}}(y, z; X)$ is the local eigenfunction of problem (2.5) and the superscripts $^-$ and $^+$ refer to the region upstream and downstream of the saddle point X_s, respectively.

The identification of the unstable global eigenvalue ω_G associated with the self-sustained flow oscillations is one of the main objectives of a global stability analysis. In order to obtain an accurate estimation of ω_G by local analysis, the correction term $\epsilon\omega_\epsilon$ in (2.7) can be also considered.

In a small region of size $O(\epsilon^{1/2})$ around the turning point X_s, the WKBJ approximation breaks down. If a new inner streamwise scaling $\bar{X} \equiv (X - X_s)\epsilon^{-1/2}$ is considered, the perturbation in the region near X_s can be sought in the following form:

$$\bar{\boldsymbol{q}} \sim \bar{A}(\bar{X}) \exp\left[\mathrm{i}\epsilon^{-1}k_{0,s}(X - X_s)\right], \tag{2.9}$$

where $k_{0,s} = k_0(X_s)$ and the amplitude $\bar{A}(\bar{X})$ is found by imposing a suitable orthogonality condition (Fredholm alternative) at higher order (see Huerre & Monkewitz 1990). Lastly, the eigenvalue correction term ω_ϵ is evaluated by the asymptotic matching of the outer WKBJ solution with the inner expansion that is valid in the double turning point region. In particular, ω_ϵ is restricted to assume discrete values:

$$\omega_\epsilon = \left[-\frac{\mathrm{i}}{2}\omega_{kk}k_{0X} + \sqrt{\omega_{0XX}\omega_{kk}}\left(n + \frac{1}{2}\right)\right], \tag{2.10}$$

https://doi.org/10.1017/jfm.2017.167 Published online by Cambridge University Press

where n is an integer and all the quantities ($\omega_{kk} = \partial^2\omega/\partial k^2$, $k_{0X} = \partial k_0/\partial X$, $\omega_{0XX} = \partial^2\omega_0/\partial X^2$) are evaluated at the complex saddle point X_s. All terms in (2.10) can be computed from the behaviour of the dispersion relation around X_s and k_0.

In the following, the symbol $\omega_G(glob)$ denotes the complex global eigenvalue resulting from global stability analysis. The symbol $\omega_{G,0}(loc)$ denotes the global eigenvalue evaluated from the WKBJ approximation at order $O(\epsilon^0)$, which is equivalent to the saddle-point condition, i.e. $\omega_{G,0}(loc) = \omega_s$, and $\omega_{G,1}(loc)$ stands for the value at order $O(\epsilon^1)$, i.e. $\omega_{G,1}(loc) = \omega_s + \epsilon\omega_\epsilon$. Lastly, the expressions without correction and with correction will be used in the following to indicate quantities evaluated considering $\omega_{G,0}(loc)$ and $\omega_{G,1}(loc)$, respectively.

Note that (2.10) is slightly different from the equivalent expression given in Huerre & Monkewitz (1990). More precisely in (2.10) a $\delta\omega$ term is missing in comparison with equation (6.1) provided in Huerre & Monkewitz (1990) but this is not an approximation. Indeed, the term $\delta\omega$ reported in the cited paper stems from terms containing the cross-stream base flow velocity components, V_b and W_b, and the streamwise derivative of the horizontal velocity component, $\partial U_b/\partial X$; moreover, it collects effects coming from the viscous perturbation terms (see equation (A10) in Monkewitz *et al.* (1993)). As already discussed, in our approach these terms have been retained in the leading order (2.5), so that their effect is automatically included in the analysis. In general, the terms mentioned above are not negligible if an accurate estimate of the global frequency is sought. As an example we estimated in § 4.3 the effect of the non-parallel terms containing V_b and W_b and $\partial U_b/\partial X$ on the corrected frequency $\omega_{G,1}(loc)$ for the incompressible flow over a sphere at flow Reynolds number $Re = 275$. Estimation is obtained by subtracting the value of $\omega_{G,1}(loc)$ obtained by alternately including and neglecting such terms in (2.5), and the results provided in the referenced section demonstrate that the contribution of the non-parallel terms is important for an accurate estimation of $\omega_{G,1}(loc)$. Unfortunately, we could not follow the same procedure in estimating the effects of the viscous terms, since neglecting them in (2.5) would lead to a singular problem with the need to use a rational asymptotic approach (or multi-deck expansion). A more detailed discussion on this issue can be found in Giannetti & Luchini (2006).

Concerning (2.10), it is possible to notice that it predicts a series of global modes, one for each value of the free integer parameter n. Here we consider only the first one ($n = 0$), since this is the most unstable one: the higher modes are, in fact, more damped, since the imaginary part of the term $(\omega_{0XX}\omega_{kk})^{0.5}$ is negative.

In conclusion, we remark that the previous analysis is based on a linear framework and is therefore valid for infinitesimal perturbations close to the critical point. When nonlinear and saturation effects become significant the spatial structure of the mode can be recovered by a nonlinear temporal direct numerical simulation (DNS) or, in a weakly non-parallel setting, by using the elephant modes theory developed by Pier *et al.* (1998) and Pier & Huerre (2001).

3. Numerical approach

Direct numerical simulations documented here are carried out using Nek5000 (http://nek5000.mcs.anl.gov), which is a spectral-element code based on Lagrange polynomial interpolants in the $P_N - P_{N-2}$ formulation, based on tensor-product arrays of Gauss–Lobatto–Legendre (GLL) quadrature points in each hexahedral element. A third-order backward differentiation formula is used for the time discretisation; the viscous terms are treated implicitly and the convective ones explicitly by a third-order forward extrapolation.

https://doi.org/10.1017/jfm.2017.167 Published online by Cambridge University Press

In global stability analysis, the linearised direct and adjoint Navier–Stokes equations for a small-amplitude disturbance are solved using Nek5000. The code is used as a time stepper and it is coupled with the IRAM eigenvalue solver implemented in ParPACK (see e.g. Lashgari *et al.* 2014; Tammisola *et al.* 2014). For the local stability analysis, spatial discretisation is obtained by Taylor–Hood finite elements using the code FreeFem++ (http://www.freefem.org). Both the resulting temporal and spatial stability problems are solved by a Krylov–Schur method with a shift–invert technique, using the implementation already available in the SLEPc library (http://slepc.upv.es). Higher-order WKBJ correction terms can be included to increase the accuracy of the approximation. In particular, the eigenvalue correction ω_ϵ can be computed by evaluating the expression in square brackets in (2.10). Particular attention must be paid when evaluating such terms. Indeed, the determination of the complex saddle point and the calculation of the other terms appearing in (2.10) must be performed by analytic continuation of the dispersion relation in the complex X plane. This procedure is generally performed by fitting the available data with a simple polynomial (Pier 2002) or rational function (Cooper & Crighton 2000) and successively by evaluating the interpolant for complex X values. While the leading-order term ω_s has been evaluated without problems by several authors by using different procedures, the choice of an appropriate interpolation/extrapolation technique becomes crucial to accurately evaluating the correction ω_ϵ. This term is in fact small compared with ω_s so that special attention must be paid in selecting a procedure that minimises high-frequency errors. The presence of such components can, in fact, lead to errors even larger than the correction itself. In this paper, we adopted a particularly accurate reconstruction procedure. Firstly, the data available for real X values are fitted using cubic splines in order to smooth out the high-frequency error terms. Secondly, Chebyshev rational approximation is used for the function reconstruction in the complex X plane as implemented in the Matlab library Chebfun (http://www.chebfun.org). The resulting procedure allows for an accurate determination of the global eigenvalue ω_G. As regards the spatial shape of the associated global mode, this can be determined by inspecting (2.8); non-parallel effects can be taken into account by the amplitude function $A(X)$ which can be determined by solving the compatibility equation for the second-order WKBJ approximation.

4. Results

In this section, we show the results obtained in estimating the stability properties of a globally unstable flow using the local stability analysis as illustrated in § 2. To achieve this, we consider three different flow configurations: the two-dimensional flow past a circular cylinder, the laminar boundary layer (BL) flow over a hemispherical roughness element placed on a flat plate and the flow past a fixed sphere positioned in a uniform stream. The flow past a circular cylinder is a well-documented case in the literature and, for this reason, it also provides us with a validation of the used tools. Conversely, the other two cases are fully three-dimensional complex flow configurations. Results pertaining to the considered flow configurations are discussed in the following sections.

4.1. *Flow past a circular cylinder*

The two-dimensional flow past a circular cylinder is considered here. All flow quantities are normalised using the uniform incoming velocity U_∞ and the diameter D of the cylinder, which are the reference quantities used for the definition of the

https://doi.org/10.1017/jfm.2017.167 Published online by Cambridge University Press

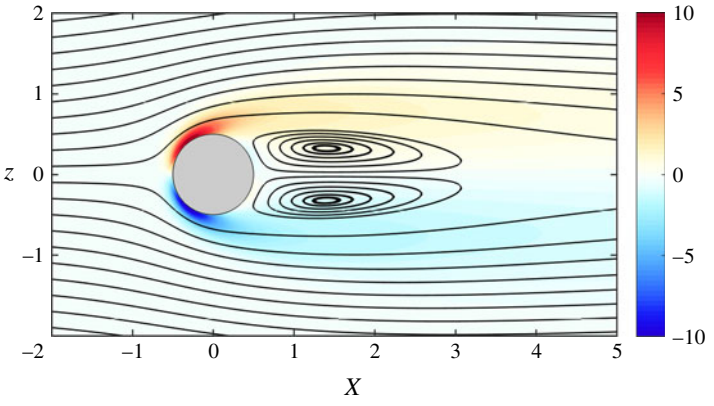


FIGURE 1. (Colour online) Vorticity (colour) and streamlines of the flow past the circular cylinder at $Re = 50$ (streamline spacing in the z-direction is $0.2D$ outside the separation bubble and $0.04D$ in the recirculating region).

flow Reynolds number. Considering a frame of reference with the origin on the cylinder axis, the x-axis parallel to the free-stream velocity and the z-axis with the cross-stream velocity (see for instance figure 1), the dimensions of the computational domain used are the following: $-15 \leqslant x/D \leqslant 35$ and $-15 \leqslant z/D \leqslant 15$. The velocity is imposed at the inflow ($x/D = -15$), while stress-free conditions are applied on the lateral boundaries ($z/D = \pm 15$) and on the outflow boundary ($x/D = 35$).

The two-dimensional base flow is computed using Nek5000 and employing about 1500 spectral elements of degree $N_p = 7$. The same grid is also used for the global stability analysis so as to characterise the onset of the primary instability. In particular, the predicted value of the critical Reynolds number is equal to $Re_{cr} \simeq 46.2$, which is in close agreement with the literature. For instance, in Giannetti & Luchini (2007) Re_{cr} is estimated to be $Re_{cr} \simeq 46.7$.

In order to show how the improved local stability analysis (with second-order correction effects included) performs in estimating the global stability properties, we consider the flow in supercritical conditions at $Re = 50$. The corresponding unstable steady state is depicted in figure 1, where the streamline pattern around the cylinder is shown together with vorticity along the y axis. The global stability analysis using Nek5000 as a time stepper identifies the leading unstable global eigenvalue, $\omega_G(glob) = 0.759 + 0.016\mathrm{i}$, which is in good agreement with Giannetti & Luchini (2007), as reported in table 1 for comparison.

When standard local analysis, i.e. without correction, is applied following the indications provided in § 2.2, a region of absolute instability, i.e. where $\omega_{0,i}(X) > 0$, is found in the near wake of the cylinder (not shown here for brevity), which extends in the streamwise direction up to $X \simeq 3.8$. Since an analytical continuation of the local absolute frequency in the complex X-plane is required, the curve $\omega_0(X)$ is first interpolated with cubic splines to smooth out the numerical data and then analytically continued from the real X-axis into the complex space using an accurate Chebyshev rational polynomial approximation of order N. The saddle point is then identified using a Newton method, for values of N ranging from 6 to 12 and no significant variations of the X_s and ω_s are found. For instance, the estimated values of X_s and ω_s for a progressive increase of the polynomial order N from $N = 5$ to $N = 9$ are reported in the first two rows of table 2. As it can be evinced from table 2, no significant

https://doi.org/10.1017/jfm.2017.167 Published online by Cambridge University Press

	Reference	ω_g	$\lvert\omega_{ref}-\omega\rvert/\lvert\omega_{ref}\rvert$ (%)
Global analysis	Present $\omega_G(glob)\equiv\omega_{ref}$	$0.759+0.016\mathrm{i}$	—
	Giannetti & Luchini (2007)	$0.750+0.013\mathrm{i}$	0.4
Local analysis	Pier (2002)	$0.785+0.091\mathrm{i}$	10.9
	Juniper & Pier (2015)	$0.791+0.083\mathrm{i}$	10.4
	Present $\omega_{G,0}(loc)$	$0.750+0.084\mathrm{i}$	9.1
	Present $\omega_{G,1}(loc)$	$0.729+0.012\mathrm{i}$	3.1

TABLE 1. Flow past a circular cylinder at $Re=50$: globally unstable eigenvalue and its prediction by corrected and uncorrected local stability analysis.

	$N=5$	$N=7$	$N=9$
X_s	$+2.1130+0.8590\mathrm{i}$	$+2.1109+0.8613\mathrm{i}$	$+2.1110+0.8628\mathrm{i}$
$\omega_{G,0}(loc)=\omega_s$	$+0.7497+0.0842\mathrm{i}$	$+0.7498+0.0842\mathrm{i}$	$+0.7498+0.0842\mathrm{i}$
$\omega_{G,1}(loc)=\omega_s+\epsilon\omega_\epsilon$	$+0.7298+0.0100\mathrm{i}$	$+0.7289+0.0126\mathrm{i}$	$+0.7294+0.0113\mathrm{i}$
ω_{0XX}	$+0.0271-0.0582\mathrm{i}$	$+0.0261-0.0573\mathrm{i}$	$+0.0261-0.0567\mathrm{i}$
ω_{kk}	$-0.1679-0.5686\mathrm{i}$	$-0.1703-0.5496\mathrm{i}$	$-0.1664-0.5699\mathrm{i}$
k_{0K}	$+0.1100-0.0486\mathrm{i}$	$+0.1113-0.0496\mathrm{i}$	$+0.1106-0.0489\mathrm{i}$

TABLE 2. Estimation of coefficients in (2.10) (ω_{0XX}, ω_{kk}, k_{0K}) and of the complex global eigenvalues at different order of approximation ($\omega_{G,0}(loc)$, $\omega_{G,1}(loc)$) with increasing values of N, i.e. the order of rational function used for continuation in the complex plane.

discrepancies are shown by varying the order of the polynomial extrapolation in the considered range. Moreover, following the indications provided in Juniper & Pier (2015), the numerical convergence in the estimation of X_s and ω_s have been appraised by progressively including all points that satisfy the condition $\omega_{0,i}>\xi$, varying ξ from 0.1 to -0.1. This convergence test, whose results are not reported here for brevity, substantially confirmed that the values reported in table 2 are converged with a discrepancy which is less than 2 % for all the considered cases.

The position of the complex saddle point is found at $\omega_s=\omega_{G,0}(loc)=0.750+0.084\mathrm{i}$, $X_s=2.112+0.863\mathrm{i}$. These results are in agreement with Pier (2002), Juniper & Pier (2015), as can be also evinced by table 1, thus validating the procedure and the numerical tools used for this study. The local approach predicts the global unstable eigenvalue with an error of 9.1 %. In this particular case, the error is larger for the complex part of the unstable eigenvalue, i.e. for the temporal growth factor. As a consequence, the standard local stability analysis estimates the critical Reynolds number $Re_{cr}\simeq 27.3$, which differs significantly from the value determined by a global stability analysis, with a percentage error of about 42 %.

The results of the local stability analysis can be corrected as detailed in § 2.2. To do this, the coefficients in (2.10) have to be evaluated at the complex saddle point X_s. To check the numerical convergence in the estimation of the mentioned coefficients and of $\omega_{G,1}(loc)$, these quantities have been evaluated for increasing values of the order N of the adopted rational function for continuation in the complex pane (see § 3 for details), and results, reported in table 2, demonstrate a substantial convergence.

Applying (2.10), the resulting corrected eigenvalue is equal to $\omega_{G,1}(loc)=0.729+0.012\mathrm{i}$, demonstrating the efficacy of the correction which in this case decreases the

https://doi.org/10.1017/jfm.2017.167 Published online by Cambridge University Press

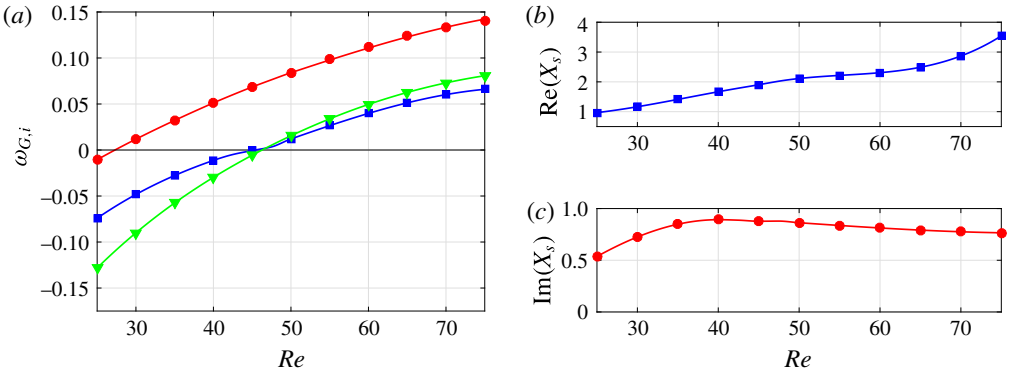


FIGURE 2. (Colour online) (*a*) Estimation of the Re_{cr} for the primary wake instability of the flow past a circular cylinder. Green triangles: global stability analysis; red circles: local stability analysis not corrected; blue squares: local stability analysis with correction. Spatial position of the saddle point with Re: real (*b*) and imaginary (*c*) part of X_s, obtained considering a rational function of $N = 7$ for continuation in the complex plane.

error with respect to global stability analysis to approximately 3 %, as also reported in table 1. In particular, the accuracy of the predicted growth factor is greatly improved by the proposed correction, thus leading to an accurate estimation of Re_{cr}, i.e. $Re_{cr} \simeq 45.2$, which compares well with the true value, the discrepancy being of approximately 3.2 %.

As a further assessment of the beneficial effects of the proposed correction, we report in figure 2(*a*) the values of the global growth rate estimated by the local stability analysis with and without correction, i.e. $\omega_{G,1}(loc)$ and $\omega_{G,0}(loc)$ respectively, in comparison with the equivalent values estimated by the global stability analysis, for values of Reynolds number ranging from $Re = 25$ to $Re = 75$. The figure clearly shows that the applied correction systematically improves the predictions of the local stability analysis over the range of Reynolds numbers considered and, as already commented, significantly improves the prediction of the critical conditions for the onset of the wake instability. In addition, the position of the saddle point X_s as a function of the Reynolds number is also reported in figure 2(*b*,*c*). Since the length of the recirculation region in the near wake of the cylinder increases with the flow Reynolds number, the saddle point moves slightly downstream, i.e. Re(X_s) increases. In contrast, the distance of X_s from the real X-axis, i.e. Im(X_s), remains substantially unchanged, at least for the considered range of Reynolds numbers.

4.2. *Flow past a wall-mounted hemispherical roughness element*

In this section we consider the three-dimensional flow over a wall-mounted roughness element which is positioned inside an incoming laminar boundary layer (BL). The considered configuration is sketched in figure 3(*a*,*b*) together with the considered Cartesian coordinate system. The roughness element is composed by a hemisphere of radius R connected to the wall by a thin circular cylinder with the same radius and a height of $h = 0.1R$ (for further geometrical details see Citro *et al.* 2015). In this case, the Reynolds number, Re_k, is based on the total height k of the obstacle (see figure 3*b*) and the flow velocity U_k, i.e. the streamwise velocity that we would be measured at point $(x = 0,\ y = k)$ in the absence of the hemispherical obstacle. All quantities

https://doi.org/10.1017/jfm.2017.167 Published online by Cambridge University Press

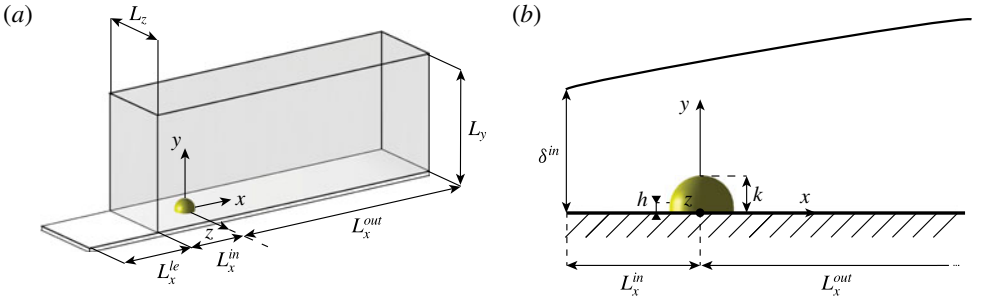


FIGURE 3. (Colour online) Flow past a wall-mounted hemispherical roughness: configuration and frame of reference (not in scale).

reported in the following in non-dimensional form are normalised using k and U_k as reference length and velocity. With reference to figure 3(*a*), the computational domain is characterised by $L_x^{in} = 7R$, $L_x^{out} = 30R$, $L_y = 8R$, $L_z = 10R$ (labelled $M1$ in Citro *et al.* (2015)) and the inherent mesh has approximately 9×10^3 spectral elements. Validation and convergence tests are reported in section 2D in Citro *et al.* (2015). Concerning the boundary conditions for the DNS, null velocity ($\boldsymbol{u} = (0, 0, 0)$) is imposed at the solid boundaries, a fully developed Blasius BL velocity profile is imposed at the inlet of the domain and, finally, stress-free conditions, i.e. $p\boldsymbol{n} - Re^{-1}\boldsymbol{\nabla u} \cdot \boldsymbol{n} = 0$, are imposed on the remaining boundaries.

For this flow configuration, the results from the WKBJ at higher order are presented and compared with those obtained by the global analysis for $Re_k = 450$ (see Citro *et al.* 2015). The wall-normal vorticity and the velocity streamlines of the unstable base flow in the near wake of the roughness element are reported in figure 4. At this value of Re_k, the flow is characterised by the shedding of periodic hairpin vortices inside the BL, with a Strouhal number $St = \omega k/2\pi U_k \simeq 0.16$ (for further details, see Citro *et al.* 2015). As reported in figure 5(*a*), the streamwise evolution of the absolute growth rate $\omega_{0,i}$ shows that the flow is absolutely unstable in the region $0.77 < X < 1.73$. This is in reasonable agreement with the dimensions of the recirculation region in the near wake of the hemispherical element, that extends in streamwise direction up to $X = 1.9$ (see figure 4).

Following the same procedure detailed in § 4.1 for the circular cylinder, the saddle point is found for $\omega_s = \omega_{G,0}(loc) = 1.6322 + 0.1994\mathrm{i}$ and $X_s = 1.2923 - 0.047\mathrm{i}$. For a further verification, the location (ω_s, X_s) is found by a graphical method seeking the cusp point in the ω_0-plane. Referring to figure 5(*b*), the streamwise evolution of ω_0 is plotted at different values of the imaginary part of the complex X-plane, $X_{s,i}$. The saddle point is then identified by the values for which a cusp formation is visible in the absolute frequency plane. The global analysis identifies, for this flow configuration, a reference complex eigenvalue equal to $\omega_G(glob) = 1.858114 + 0.087148\mathrm{i}$ (Citro *et al.* 2015), which is slightly more stable than the one estimated by local analysis. However, the over-prediction of the global growth rate is a common characteristic of the local analysis, as already highlighted, for example, in Juniper *et al.* (2011). Lastly, the correction in (2.10) is considered in order to obtain a more accurate estimate of the global eigenvalue, taking into account the correction term ω_ϵ in the WKBJ expansion at order $O(\epsilon^1)$. In particular, following the same extrapolation procedure used for the circular cylinder flow configuration presented in § 4.1, the resulting complex global frequency is found equal to $\omega_{G,1}(loc) = 1.6781 + 0.0376\mathrm{i}$. This result shows that, for

https://doi.org/10.1017/jfm.2017.167 Published online by Cambridge University Press

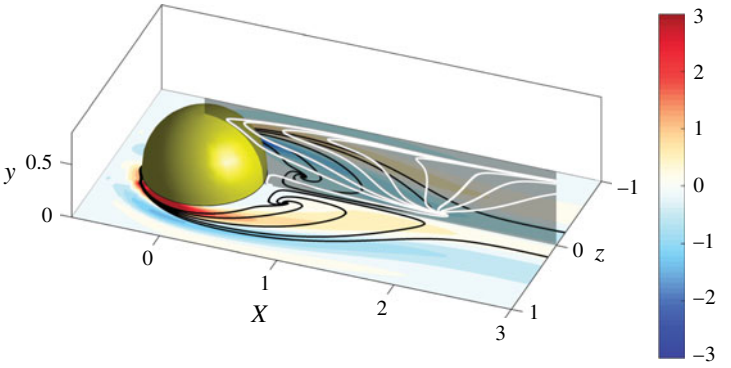


FIGURE 4. (Colour online) Streamlines of the flow past the hemispherical roughness element at $Re_k = 450$ in the planes $y = 0.03$ and $z = 0$. Colour contours depict the wall-normal vorticity in the plane $y = 0.03$.

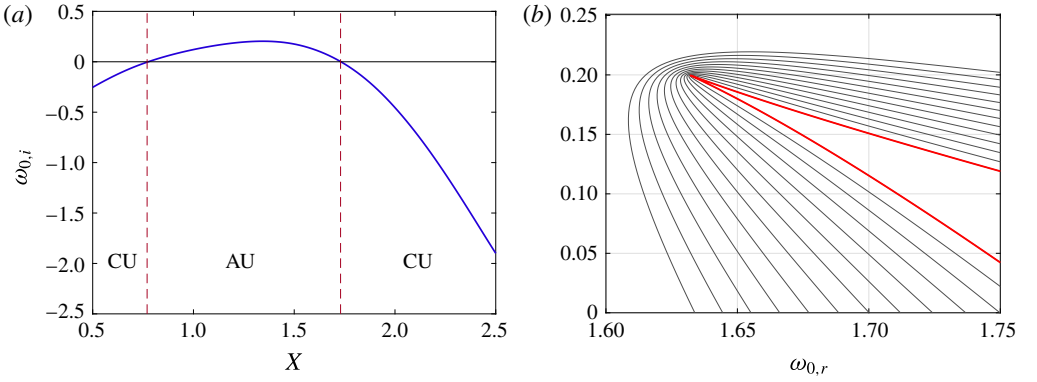


FIGURE 5. (Colour online) (*a*) Spatial evolution of the absolute growth rate ω_{0i} (CU = convectively unstable flow, AU = absolutely unstable flow); (*b*) evolution of ω_0 for different values of the complex X obtained with a seventh-order rational function for continuation in the complex plane. The red line corresponds to the saddle-point value, $\mathrm{Im}(X) = -0.047$ and the successive lines are evaluated at different values of $\mathrm{Im}(X)$, with steps equal to -0.009.

this specific case, the correction procedure leads to an improved estimation of the global eigenvalue, especially of its imaginary part, which is related to the frequency in time of the global mode. For the sake of completeness, the correction coefficients in (2.10), using $N = 7$ as the order of the rational function, are: $\omega_{0XX} = 1.8418 - 1.6684\mathrm{i}$, $\omega_{kk} = 0.0235 - 0.0715\mathrm{i}$, $k_{0K} = 1.6445 - 1.0907\mathrm{i}$.

4.3. *Flow past a fixed sphere*

In this section, we detail the numerical results obtained for a sphere of radius R positioned in a uniform incompressible flow. Figure 6 depicts the flow configuration and the frame of reference adopted in the present study. The reference quantities for the normalisation of the flow quantities and for the definition of the flow Reynolds number, Re_D, are the sphere diameter D and the uniform streamwise velocity U_∞. The same flow configuration has been characterised by DNS and global stability

https://doi.org/10.1017/jfm.2017.167 Published online by Cambridge University Press

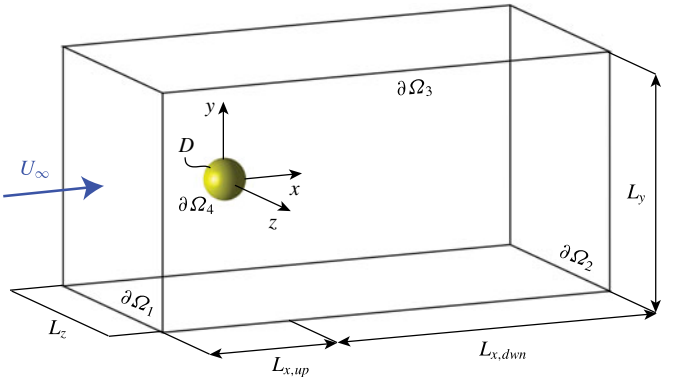


FIGURE 6. (Colour online) Flow past a spherical body: configuration and frame of reference (not to scale).

analysis in Citro *et al.* (2016) and we use here the same computational domain and discretisation parameters adopted in that paper. With reference to figure 6, the dimensions of the computational domain used for both the simulation and the global stability analysis are: $L_{x,up} = 12$, $L_{x,dwn} = 35$, $L_y = 24$, $L_z = 24$; the mesh is made by approximately 1.3×10^4 spectral elements of degree $N_p = 13$. On both the inlet boundary $\partial\Omega_1$ and the lateral boundaries $\partial\Omega_3$ a constant velocity profile is imposed, which is parallel to the x axis, and a stress-free condition is imposed on the outlet boundary $\partial\Omega_2$. Validation and convergence tests leading to the adopted choice of the numerical discretisation are detailed in Citro *et al.* (2016). Here we focus our attention on the occurrence of the second bifurcation that arises at $Re_D = 271.8$, which leads the flow from a steady asymmetric state to a flow configuration characterised by an asymmetric mean flow and by the time-periodic shedding of vortical structures in the wake. For $Re_D = 275$ the vortex shedding frequency in terms of the Strouhal number is equal to $St \simeq (\omega D/2\pi U_\infty) \simeq 0.13$. An example of the steady unstable flow past the sphere in supercritical conditions is given in figure 7(*a*), where the modulus of the velocity field and the velocity streamlines are shown for the section $z = 0$ (the mid-plane of the computational domain) at $Re_D = 275$.

When the global stability analysis is applied to the flow field in figure 7(*a*), a globally unstable mode is found with an associated complex eigenvalue equal to $\omega_G(glob) \simeq 0.8092 + 0.006\mathrm{i}$. The real part of the corresponding global eigenmode is plotted in figure 9(*e*,*f*).

When the classical local stability analysis is applied to the wake, i.e. considering only first-order terms in the WKBJ expansion, a region of absolute instability is identified by inspecting where the absolute growth rate $\omega_{0,i}$ is positive. As shown in figure 7(*b*), where the streamwise evolution of $\omega_{0,i}$ is depicted, the flow is absolutely unstable in the region $0.47 < X < 1.95$. The length of this region is comparable to that of the asymmetric recirculation bubble, which extends in the streamwise direction from the top of the sphere, where separation first occurs, to $X \simeq 2$ (see figure 7*a*).

As described in § 2.2, continuing $\omega_0(X)$ in the complex X plane, the eigenvalue of the globally unstable flow can be approximated at the leading order ϵ by the eigenvalue estimated at the saddle point $(\omega_s,\ X_s)$. The numerical procedure for continuation in the complex plane, already commented on in the previous sections, makes it possible to identify the saddle point at $\omega_s = \omega_{G,0}(loc) = 0.7369 + 0.2235\mathrm{i}$

https://doi.org/10.1017/jfm.2017.167 Published online by Cambridge University Press

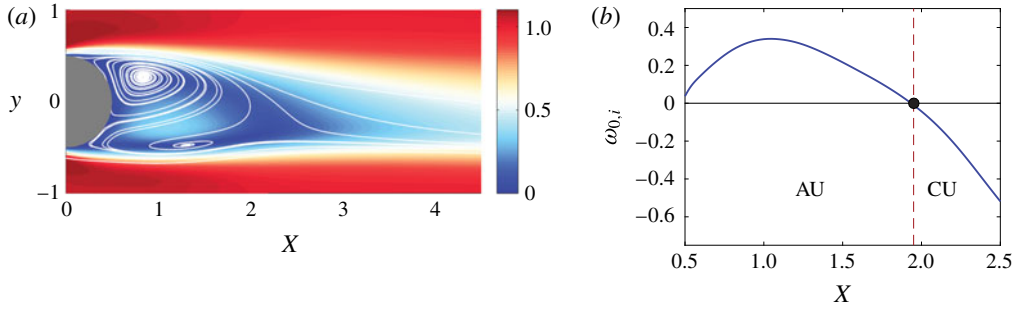


FIGURE 7. (Colour online) (*a*) Modulus of velocity (colour) and streamlines of the flow past a sphere at $Re_D = 275$ in the midplane ($z = 0.0$); (*b*) spatial evolution of the absolute growth rate $\omega_{0,i}$ (CU = convectively unstable flow, AU = absolutely unstable flow).

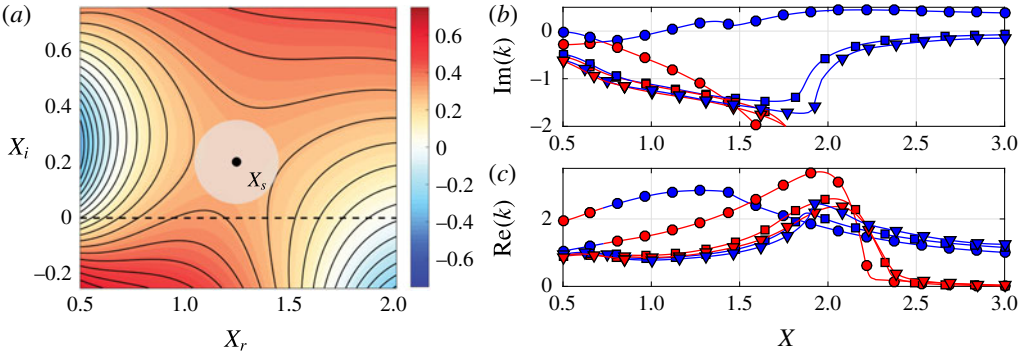


FIGURE 8. (Colour online) (*a*) Distribution of $\omega_{0,i}$ in the complex X plane. Streamwise evolution of the imaginary (*b*) and real (*c*) parts of the complex local wavenumbers k^+ (blue lines) and k^- (red lines) obtained by the local dispersion relation with $\omega = \omega_{G,0}(loc)$ (●), $\omega = \omega_{G,1}(loc)$ (■) and $\omega = \omega_G(glob)$ (▼), respectively.

and $X_s = 1.3394 + 0.2397\mathrm{i}$. This is shown in figure 8(*a*), where $\omega_{0,i}$ is plotted in the complex X plane. As in the case of the circular cylinder, the error (compared to the reference quantity $\omega_G(glob) \simeq 0.8092 + 0.006\mathrm{i}$) affects both the frequency of the global mode and, more severely, the growth rate (i.e. the imaginary part of ω), which is overestimated by a factor approximately equal to 37.25. Globally, the relative error on the eigenvalue is approximately equal to 29 %.

The estimated global complex eigenvalue is then used in the local dispersion relation at different streamwise sections to evaluate the local shape of the associated global eigenmode. In this way, from (2.8) and following the indications provided by Juniper & Pier (2015), the direct mode can be reconstructed by local analysis. As a first step the spatial evolution of the complex wavenumbers $k^{\mp}$ and the corresponding local spatial eigenmode is evaluated considering the saddle-point complex frequency $\omega_{G,0(loc)}$ in the dispersion relation. This has been done by considering X-sections uniformly placed downstream the sphere with a spacing equal to $\Delta X = 0.025$. The streamwise evolution of the wavenumbers $k^{\mp}$ is shown in figure 8(*b*,*c*) with circular symbols. Starting from this result the structure of the global eigenmode is estimated using (2.8). Figure 9(*a*,*b*) shows the resulting spatial evolution of the

https://doi.org/10.1017/jfm.2017.167 Published online by Cambridge University Press

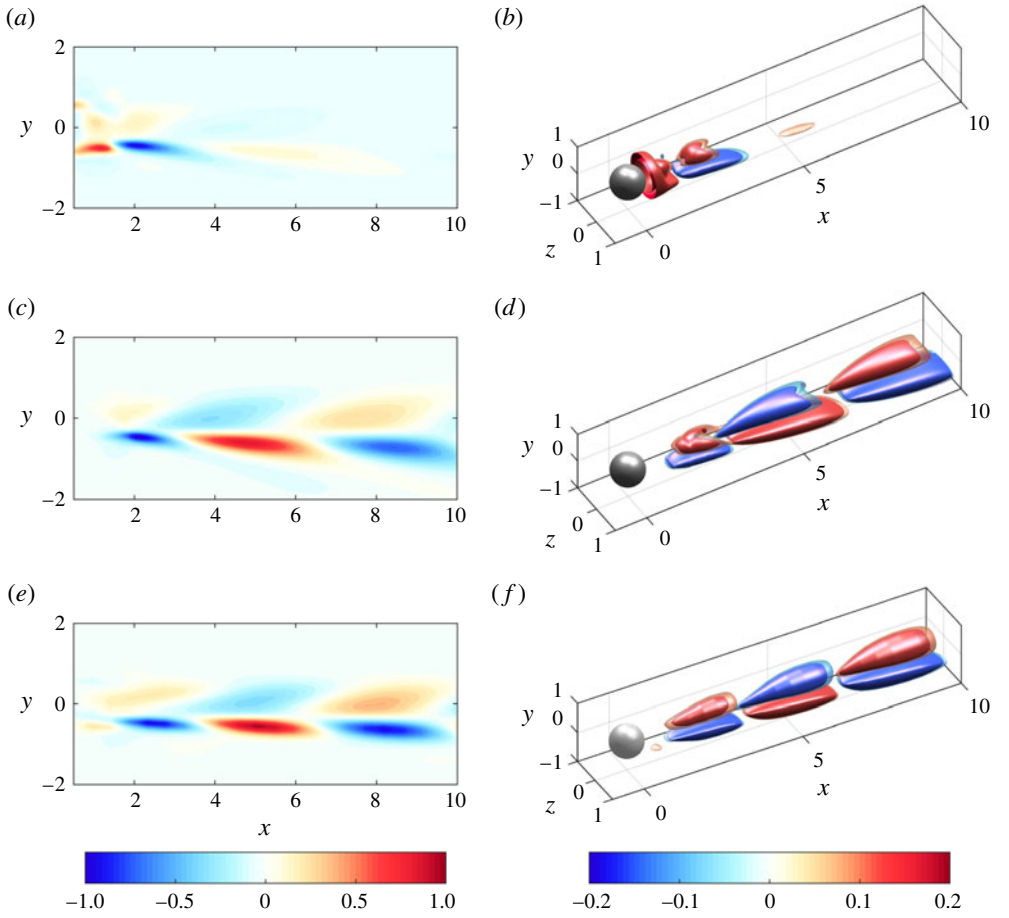


FIGURE 9. (Colour online) Real part of the leading direct global mode calculated using the standard (uncorrected) local analysis (*a*,*b*), the corrected local approach (*c*,*d*) and the global stability analysis (*e*,*f*). (*a*,*c*,*e*) Contour plot of the streamwise velocity component $\hat{u}$ in the plane ($z = 0.0$). (*b*,*d*,*f*) Perspective view of the corresponding isocontours.

velocity streamwise component of the unstable eigenmode reconstructed as described above. As can be deduced from figure 9, the standard local analysis (WKBJ at $O(\epsilon^0)$, as in Juniper *et al.* (2011)) provides a poor reconstruction of the direct mode. Indeed, the structure of the direct mode, obtained by the standard local analysis and depicted in figure 9(*a*,*b*), is very different from the reference one obtained by global stability analysis and depicted in figure 9(*e*,*f*).

In order to highlight the beneficial effects that can be obtained by the proposed correction, the local analysis is now repeated for the same flow including the higher-order terms in the WKBJ expansion (WKBJ at $O(\epsilon^1)$). As a first result the corrected global eigenvalue is now equal to $\omega_{G,1(loc)} = 0.7898 + 0.0266\mathrm{i}$. The percentage error with respect to the reference value obtained by global stability analysis is now reduced to 4 %; it was approximately equal to 29 % without including higher-order terms. For sake of completeness we also provide the coefficients used in (2.10) so as to estimate the global eigenvalue with the higher-order correction: $\omega_{0X} = 0.7042 - 0.1965\mathrm{i}$, $\omega_{kk} = -0.1334 - 0.3333\mathrm{i}$ and $k_{0X} = 0.9252 + 0.6703\mathrm{i}$.

https://doi.org/10.1017/jfm.2017.167 Published online by Cambridge University Press

The present test case has also been used to appreciate the importance of retaining the non-parallel terms containing V_b and W_b and $\partial U_b/\partial X$ in the estimation of the corrected frequency $\omega_{G,1}(loc)$. As discussed in § 2.2, the inclusion of the mentioned terms is equivalent to the explicit inclusion of the term $\delta\omega$ appearing in Huerre & Monkewitz (1990) (see equation (6.1) of the cited reference) in the estimation of $\omega_{G,1}(loc)$. In our case the term $\delta\omega$ is evaluated by subtracting the value of $\omega_{G,1}(loc)$ obtained by alternately including and neglecting the mentioned non-parallel terms in (2.5). As a result, it is found that $\delta\omega \approx 0.1963 + 0.0829i$, which is not negligible if compared with the estimated global eigenvalue $\omega_{G,1(loc)} = 0.7898 + 0.0266\mathrm{i}$.

Besides the error reduction in the estimation of the global eigenvalue, the proposed correction can also lead to a significant improvement in the estimation of the spatial shape of the corresponding eigenmode. In particular, as remarked above, a solution which is accurate up to order $O(\epsilon)$ can be obtained by determining the slowly evolving function $A(X)$ and by computing the global mode shape with the corrected eigenvalue $\omega_{G,1(loc)}$, as expressed in the following, using the same conventions and notation proposed in Juniper *et al.* (2011):

$$\hat{\boldsymbol{q}}(x, y, z) \sim A(X)^{\mp}\hat{\boldsymbol{q}}(y, z; X)\exp\left[\mathrm{i}\epsilon^{-1}\int_{X_s}^{X} k^{\mp}(\omega_{G,1}(loc); X')\,\mathrm{d}X'\right], \tag{4.1}$$

where the local wavenumbers $k^{\mp}$ are now evaluated considering $\omega_{G,1}(loc)$ in the dispersion relation. Their resulting streamwise evolution is depicted in figure 8(*b*,*c*) using square symbols. For comparison, in the same figures we report the same branches $k^{\mp}$ evaluated by forcing $\omega_G(glob)$ in the dispersion relation (with triangle symbols) and evaluated by forcing $\omega_{G,0}$ (circular symbols). For the sphere case, a marked improvement is already obtained by just recomputing the eigenfunction shape, using the corrected frequency $\omega_{G,1}(loc)$ in the dispersion relation and without including the slow amplitude function $A(X)$. With this aim, figure 9(*c*,*d*) shows the spatial distribution of the streamwise velocity component of the unstable mode retrieved using the corrected eigenvalue $\omega_{G,1}(loc)$. As can be deduced from figure 9, the mode obtained using the present approach is in excellent agreement with the corresponding mode shape obtained through a fully three-dimensional global stability analysis, reported in figure 9(*e*,*f*). Note that, in a linear setting, the amplitude of the mode is undetermined, so that a normalisation must be chosen when comparing the eigenfunctions: here we used $\max|\hat{u}(x, y, z)| = 1$, while the phase was fixed at a given position in space. A further improved reconstruction, accurate up to $O(\epsilon^1)$, could be obtained by using the corrected frequency $\omega_{G,1}(loc)$ not only to evaluate the eigenfunction shape but also to evaluate the slow amplitude function $A(X)$ appearing in expression (2.8). This can be achieved by writing the solvability condition of the outer problem at order $O(\epsilon^1)$: for details on the derivation and practical implementation of the solvability condition we refer the interested reader to Zuccher & Luchini (2014) and Giannetti & Luchini (2006): the resulting linear differential equation for $A(X)$ can be readily solved to provide, together with (4.1), an approximation of the eigenmode which is accurate up to $O(\epsilon^1)$. Here we did not evaluate the amplitude $A(X)$, since in this case the correction can expected to be very small (not appreciable from a graphical point of view) and the reconstruction based on the corrected frequency $\omega_{G,1}(loc)$ already provides excellent results.

https://doi.org/10.1017/jfm.2017.167 Published online by Cambridge University Press

5. Summary

In this paper, we show that the classical local spatio-temporal stability analysis of weakly non-parallel flows can be straightforwardly applied to investigate slowly evolving three-dimensional flows, thus generalizing the Orr–Sommerfeld equations so as to include this class of cases. Moreover, we show that the inclusion of higher-order terms in the WKBJ analysis is a crucial ingredient in obtaining results which compare quantitatively well with those provided at definitely higher computational costs through global stability analysis. In particular, in this paper, we first consider the flow past a circular cylinder, since this is a well-documented case in the literature. Previous numerical studies documented in literature (Giannetti & Luchini 2007) showed that the simple local analysis at order $O(\epsilon^0)$ fails to predict the critical Reynolds number for such flow. We show here that the inclusion of $O(\epsilon^1)$ terms reduces the relative error on the critical Reynolds number from 42 % to 3.2 %.

After having considered the well-known flow past a circular cylinder, used here as a validation case of the proposed approach, we show that an equivalent improvement in the prediction of the global stability properties is obtained for two fully three-dimensional flow configurations, i.e. the boundary layer flow past a wall-mounted hemispherical obstacle and the secondary instability of the wake past a sphere. In both cases, the complex eigenvalues evaluated by the proposed local approach are in good agreement with the reference ones obtained by the global stability analysis and markedly improved if compared with the results that can be obtained by classical local analysis. In this paper, it is shown that the proposed correction for the local analysis also significantly improves the prediction of the globally unstable eigenmode and not only the associated eigenvalue. An example is provided for the wake past a sphere, for which it is shown that the eigenmode predicted by the corrected local analysis is in excellent agreement with the reference mode obtained by global analysis. In contrast, the eigenmode predicted by the classical (uncorrected) local analysis is markedly different and, thus, liable to large errors. The limitations of the approach are those common to local analysis, i.e. in principle it is not applicable to flows which are not slowly evolving in the streamwise direction; however, it is shown in the literature, as highlighted in the introduction, that the analysis provides accurate results even if the assumption of weak non-parallelism is not fully satisfied, as happens for near-wake regions past bluff bodies. In conclusion, the present study confirms that a reasonably good estimation of the global mode characteristics can be obtained just by relying on a local stability approach, if properly corrected as proposed here, with a resulting computational cost which is orders of magnitude lower than that necessary for a fully three-dimensional global stability analysis.

REFERENCES

BENDER, C. M. & ORSZAG, S. A. 1978 *Advanced Mathematical Methods for Scientists and Engineers*. McGraw-Hill.

BERS, A. 1983 Space–time evolution of plasma instabilities-absolute and convective. In *Handbook of Plasma Physics,* vol. 1, pp. 451–517. McGraw-Hill.

BRIGGS, J. 1964 *Electron–Stream Interaction with Plasmas*. MIT Press.

CHOMAZ, J. M., HUERRE, P. & REDEKOPP, L. G. 1988 Bifurcations to local and global modes in spatially developing flows. *Phys. Rev. Lett.* **60**, 25–28.

CITRO, V., GIANNETTI, F., LUCHINI, P. & AUTERI, F. 2015 Global stability and sensitivity analysis of boundary-layer flows past a hemispherical roughness element. *Phys. Fluids* **27**, 084110.

https://doi.org/10.1017/jfm.2017.167 Published online by Cambridge University Press

CITRO, V., TCHOUFAG, J., FABRE, D., GIANNETTI, F. & LUCHINI, P. 2016 Linear stability and weakly nonlinear analysis of the flow past rotating spheres. *J. Fluid Mech.* **807**, 62–86.

COOPER, A. J. & CRIGHTON, D. G. 2000 Global modes and superdirective acoustic radiation in low-speed axisymmetrics jets. *Eur. J. Mech. (*B*/Fluids)* **19**, 559–574.

GIANNETTI, F. & LUCHINI, P. 2006 Leading-edge receptivity by adjoint methods. *J. Fluid Mech.* **547**, 21–53.

GIANNETTI, F. & LUCHINI, P. 2007 Structural sensitivity of the first instability of the cylinder wake. *J. Fluid Mech.* **581**, 167–197.

HUERRE, P. & MONKEWITZ, P. A. 1985 Absolute and convective instabilities in free shear layers. *J. Fluid Mech.* **159**, 151–168.

HUERRE, P. & MONKEWITZ, P. A. 1990 Local and global instabilities in spatially developing flows. *Annu. Rev. Fluid Mech.* **22**, 473–537.

HUERRE, P. & ROSSI, M. 1998 Hydrodynamics instabilities in open flows. In *Hydrodynamics and Nonlinear Instabilities*, Cambridge University Press.

JUNIPER, M. P. & PIER, B. 2015 The structural sensitivity of open shear flows calculated with a local stability analysis. *Eur. J. Mech. (*B*/Fluids)* **49**, 426–437.

JUNIPER, M. P., TAMMISOLA, O. & LUNDELL, F. 2011 The local and global stability of confined planar wakes at intermediate reynolds number. *J. Fluid Mech.* **686**, 218–238.

LASHGARI, I., TAMMISOLA, O., CITRO, V., BRANDT, L. & JUNIPER, M. P. 2014 The planar *x*-junction flow: stability and control. *J. Fluid Mech.* **753**, 1–28.

MONKEWITZ, P. A., HUERRE, P. & CHOMAZ, J. M. 1993 Global linear stability analysis of weakly non-parallel shear flows. *J. Fluid Mech.* **251**, 1–20.

PIER, B. 2002 On the frequency selection of finite-amplitude vortex shedding in the cylinder wake. *J. Fluid Mech.* **458**, 407–417.

PIER, B. 2008 Local and global instabilities in the wake of a sphere. *J. Fluid Mech.* **603**, 39–61.

PIER, B. & HUERRE, P. 2001 Nonlinear self-sustained structures and fronts in spatially developing wake flows. *J. Fluid Mech.* **435**, 145–174.

PIER, B., HUERRE, P., CHOMAZ, J. M. & COUAIRON, A. 1998 Steep nonlinear global modes in spatially developing media. *Phys. Fluids* **10**, 2433–2435.

TAMMISOLA, O., GIANNETTI, F., CITRO, V. & JUNIPER, M. P. 2014 Second-order perturbation of global modes and implications for spanwise wavy actuation. *J. Fluid Mech.* **755**, 314–335.

THEOFILIS, V. 2011 Global linear instability. *Annu. Rev. Fluid Mech.* **43**, 319–352.

ZUCCHER, S. & LUCHINI, P. 2014 Boundary-layer receptivity to external disturbances using multiple scales. *Meccanica* **49**, 441–467.

https://doi.org/10.1017/jfm.2017.167 Published online by Cambridge University Press